## Non-Hermiticity-Governed Active Photonic Resonances

Jose D. H. Rivero, 1,2,\* Mingsen Pan, 3,\* Konstantinos G. Makris, 4,5 Liang Feng, 3,† and Li Ge, 1,2,‡

1 Department of Physics and Astronomy, College of Staten Island, CUNY, Staten Island, New York 10314, USA

2 The Graduate Center, CUNY, New York, New York 10016, USA

3 Department of Materials Science and Engineering, University of Pennsylvania, Philadelphia, Pennsylvania 19104, USA

4 Department of Physics, University of Crete, P.O. Box 2208, 71003, Heraklion, Greece

5 Institute of Electronic Structure and Laser, The Foundation for Research and Technology-Hellas, 71110 Heraklion, Greece

(Received 31 August 2020; accepted 31 March 2021; published 21 April 2021)

Photonic resonances play an essential role in the generation and propagation of light in optical and photonic devices, as well as in light-matter interaction, including nonlinear optical responses. Previous studies in lasers and other open systems have shown exotic roles played by non-Hermiticity on modifying passive resonances, defined in the absence of optical gain and loss. Here we report a new type of resonances in non-Hermitian photonic systems that does not originate from a passive resonance, identified by analyzing a unique quantization condition in the non-Hermitian extension of the Wentzel-Kramers-Brillouin method. Termed active photonic resonances, these unique resonances are found in non-Hermitian systems with a spatially correlated complex dielectric function, which is related to supersymmetry quantum mechanics after a Wick rotation. Remarkably, such an active photonic resonance shifts continuously on the real frequency axis as optical gain increases, suggesting the possibility of a tunable on-chip laser that can span a wavelength range over 100 nm.

DOI: 10.1103/PhysRevLett.126.163901

The ability to control various properties of electromagnetic waves in matter, e.g., light-matter interactions, has been the essential pursuit of optics and photonic for millennia. Classically, light-matter interactions are a result of oscillating electromagnetic fields resonantly interacting with charged particles, such as dipoles in dielectrics. In this regard, light-matter interactions can be described using a model of coupled oscillators, where the electromagnetic degree of freedom, i.e., the passive photonic mode [1], is defined by the real part of the refractive index. In a photonic environment, two types of light-matter interactions are typically defined depending on the strength of the coupling between the matter and the photonic modes, i.e., weak coupling [2–7] and strong coupling [8–15]. These two types of couplings both assume well-defined passive photonic modes, but another important matter degree of freedom, namely, non-Hermiticity (i.e., optical gain and loss), is often neglected for its seeming independence of typical resonant characteristics, including resonant frequency and mode volume.

On the other hand, balancing optical loss with gain is exactly the working principle of the laser, and hence it does not come as a surprise that the effect of non-Hermiticity on passive photonic resonances has been studied since the early days of the laser. With the exception of a bound state in the continuum [16], a passive photonic resonance in the absence of gain and loss is found in the lower half of the complex wave vector plane, i.e.,  $k = k_r + ik_i(k_i < 0)$  [17], due to the radiation loss of a laser cavity.  $|k_i|$  characterizes

the loss rate of this resonance and hence also the linewidth in the scattering spectrum of light. With the introduction of optical gain (loss), a passive resonance generally moves upward (downward) in the complex-*k* plane [Fig. 1(a)], reflecting its reduced (increased) overall loss.

There are, however, inspiring anomalies to this rule. One such behavior is on display when the system is close to an exceptional point [18–22], a non-Hermitian degeneracy where two or more passive resonances become the same. Their strongly curved trajectories [Fig. 1(b)] indicate a nonmonotonic dependence of the overall loss on the applied gain [23], leading to gain suppressed lasing [24,25] and lossinduced lasing [26]. Despite such intriguing behaviors, the role of non-Hermiticity in these and other optical systems (including gain guided lasers; see Supplemental Material [27]) is restricted to perturbing passive photonic resonances, while the exploration of observable resonances of a different origin has not been carried out. These resonances, if they exist, must arise from a fundamentally different quantization condition enabled by the presence of gain and loss, which has so far been elusive.

In this Letter, we report a new type of resonances in non-Hermitian photonic systems that does not originate from a passive resonance, identified by analyzing the non-Hermitian extension of the Wentzel-Kramers-Brillouin (WKB) method with a complex dielectric function. Termed active photonic resonances, these unique resonances are real valued and found in optical cavities featuring a dielectric function with spatially correlated real and

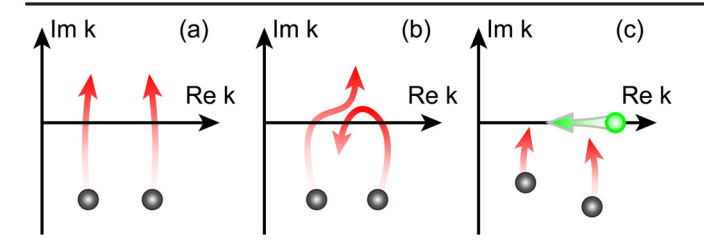


FIG. 1. Schematic trajectories of passive and active resonances with increasing gain. (a),(b) Passive resonances with spatially uniform and nonuniform gain, respectively. (c) An active resonance on the real axis versus passive resonances below the real axis.

imaginary parts. Utilizing a technique similar to the Wick rotation that transforms the Minkowski space to the Euclidean space [31], we further relate such optical cavities to supersymmetry quantum mechanics [32] and the quantum harmonic oscillator. Remarkably, such an active photonic resonance is governed by non-Hermiticity and exhibits a categorically different trajectory on the complex frequency plane, moving on the real frequency axis as optical gain increases [green dot in Fig. 1(c)].

Based on this observation, we propose a frequency tunable on-chip laser in the shape of an elongated bowtie cavity, which can span a tuning range over 100 nm, in principle. Although such a tuning range has been achieved with tabletop lasers, the tuning strategies they employ cannot be applied to an integrated on-chip platform [33]. Instead, the state-of-the-art on-chip lasers use other approaches to achieve a tuning range rather limited in comparison, which are all based on modifying or selecting different passive resonances, in one way or another [34]. Our proposal here breaks free from this conventional approach, which forms an active resonance on demand via simply tailoring the spatial gain distribution of the laser cavity.

Let us start by considering a one-dimensional (1D) optical cavity of length L=2a and a transverse wave  $\psi(x,t)$  in its steady state, i.e.,  $\psi(x,t)=\psi(x)e^{-i\omega t}$ . The system is described by the Helmholtz equation

$$[\partial_x^2 + \varepsilon(x)k^2]\psi(x) = 0, \tag{1}$$

where  $\varepsilon(x)$  is the dielectric function and we set the refractive index to be a constant  $n_e > 0$  outside the cavity. Below we take the speed of light in vacuum (c) to be 1 and do not differentiate the circular frequency  $\omega$  and the wave vector  $k = \omega/c$  in free space. A resonance is then defined by a solution of Eq. (1) with the outgoing boundary condition  $\psi(x) \propto e^{in_e k|x|}$  at  $x = \pm a$ , which is equivalent to a pole of the scattering (S) matrix where one eigenvalue of S diverges [23,35].

To illustrate how an active resonance emerges and differs from a passive resonance, we resort to the semiclassical WKB method in quantum mechanics [36] and analyze whether new quantization condition(s) arise in its non-Hermitian extension with a complex dielectric function. Below we take  $\varepsilon(x)$  to be frequency independent for simplicity. Denoting the wave function as  $\psi(x) = A(x)e^{ik\phi(x)}[A(x),\phi(x)\in\mathbb{R}]$ , we obtain the semiclassical WKB equation

$$i(2A'\phi' + A\phi'') = Ak(\phi'^2 - \varepsilon), \tag{2}$$

where we have omitted the second-order spatial derivative A''(x). Below we first focus on a real-valued  $\varepsilon(x) = n^2(x)$  to identify passive resonances in the absence of gain and loss, with which Eq. (2) reduces to

$$(A^2\phi')' = 0, \qquad \phi'(x) = \pm n(x).$$
 (3)

Note that the first relation in Eq. (3) is the same as in quantum mechanics, even though k here is complex, in general, due to the openness of the system. Together with the aforementioned outgoing boundary condition and assuming n(x) = n(-x), we obtain an explicit expression for the passive resonances (see Supplemental Material, Sec. II [27])

$$k \approx \frac{1}{\bar{n}L} \left( q - i \ln \frac{2q}{|\alpha|} \right),$$
 (4)

when  $|\alpha| \ll q$  and  $-\text{Im}[k] \ll \text{Re}[k]$ . Here  $q = (m+1/2)\pi$   $(m \in \mathbb{Z})$ ,  $\alpha \equiv \bar{n}an'(a)/n_e^2 \in \mathbb{R}$ , and  $\bar{n}$  is the average refractive index inside the cavity. Figure 2(a) exemplifies a cavity where Eq. (4) provides a good approximation for all passive resonances in the absence of gain and loss. They display intricate trajectories in the complex frequency plane once we increase the gain via the imaginary part of  $\varepsilon(x)$ 

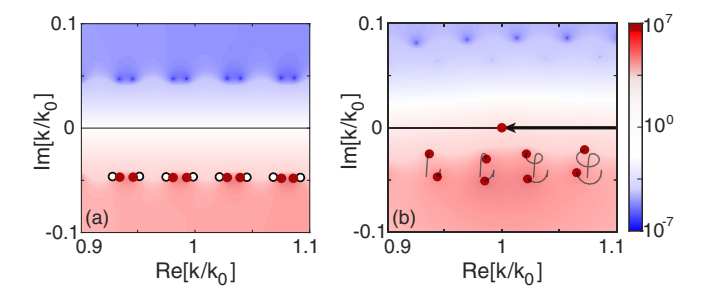


FIG. 2. Contrast between passive and active resonances. (a) Passive resonances in a cavity with  $\varepsilon(x) = (n_e x/a)^2$ . Red and white dots show the resonances and their WKB approximations, respectively. The background shows det S in the logarithmic scale. Its peaks are the poles of the S matrix marking the locations of all resonances.  $n_e = 3.3$ ,  $L = 20~\mu\text{m}$ , and  $k_0 = 2\pi/1.55~\mu\text{m}^{-1}$ . (b) Resonances and det S with  $\varepsilon(x) = (n_e x/a)^2 + i\tau n_e/a$  [see Eq. (6)], where  $\tau = k_0^{-1}$ . The black arrow and gray lines show the trajectories of the active resonance and passive resonances, respectively, when  $\tau$  increases from 0 to  $1.55/2\pi~\mu\text{m}^{-1}$ .

[Fig. 2(b)]. In stark contrast, a new type of resonance is observed: it emerges from  $+\infty$  on the real frequency axis in the Hermitian limit and red shifts with the increase of the gain.

To understand the origin of this anomalous resonance, we revisit the WKB analysis and allow the imaginary part of  $\varepsilon(x) = \varepsilon_r(x) + i\varepsilon_i(x)$  to be nonzero. Equation (3) now becomes

$$(A^{2}\phi')' = -A^{2}\varepsilon_{i}\frac{|k^{2}|}{k_{r}}, \qquad \phi'(x) = \pm \left(\varepsilon_{r} - \varepsilon_{i}\frac{k_{i}}{k_{r}}\right)^{1/2},$$

$$(5)$$

which does not lead to an explicit analytical solution in general. However, it is clear that the additional terms proportional to  $\varepsilon_i$  in Eq. (5) cause perturbations to the passive resonances, similar to the behavior observed in Fig. 2(b). More importantly, the most general form of the WKB equation here, i.e., Eq. (2), now allows a new resonance condition determined by non-Hermiticity: With the following dielectric function

$$\varepsilon(x) = w^2(x) - i\tau w'(x) \equiv \varepsilon_w(x;\tau),$$
 (6)

where  $w(x) \equiv \phi' \in \mathbb{R}$ , a new resonance is found at  $k_0 = 1/\tau \in \mathbb{C}$  that satisfies A'(x) = 0. The wave function inside the cavity is given by

$$\psi(x) = e^{ik_0 \int_0^x w(z)dz},\tag{7}$$

and the outgoing boundary condition requires  $w(\pm a) = \pm n_e$ . This wave function has a constant intensity [37–41] or phase inside the cavity if  $k_0$  is real or imaginary, respectively. For now we restrict our discussion to a real-valued  $k_0 > 0$ , which can be obtained by choosing  $\tau > 0$ . We immediately observe that it shifts on the real axis when we vary the non-Hermiticity via  $\tau$  in  $\varepsilon_w(x;\tau)$ , which explains the horizontal trajectory we have seen in Fig. 2(b), where the dielectric function is of the form given by Eq. (6) with  $w(x) = n_e x/a$ . We define this real-valued resonance as an active photonic resonance, because it does not originate from a passive counterpart in the absence of gain and loss: By taking  $\tau \to 0$ ,  $k_0$  diverges along the positive real axis, which is clearly not captured by the passive resonances in the lower half of the complex plane.

We note here that Eq. (6) resembles the two partner potentials in supersymmetric quantum mechanics [32], with one term proportional to the square of a position-dependent function and the other proportional to its spatial derivative. It turns out that a formal connection between them can be established: by substituting the free-space wave vector  $k_0$  by  $k_i = \pm ik_0$ , we effectively perform a transformation of the Helmholtz equation similar to a Wick rotation [31], changing it from Eq. (1) to

$$[-\partial_x^2 + \varepsilon(x)k_0^2]\psi(x) = 0, \tag{8}$$

which resembles the Schrödinger equation. In a Wick rotation, time is made imaginary to relate the Minkowski metric (-1, 1, 1, 1) in special relativity to the four-dimensional Euclidean metric (1,1,1,1). And here we achieve a similar transformation from the "Helmholtz metric" (1,1) to the "Schrödinger metric" (-1,1). If we define the second term in Eq. (8) as the potential V(x), then the two resulting potentials with  $k_0 \to \pm i k_0$  are given by  $V_{\pm}(x) = W^2(x) \mp$ W'(x) respectively, with  $W(x) \equiv w(x)k_0$ . They have exactly the same forms as the two partner potentials in supersymmetric quantum mechanics. Since Eq. (6) holds for any complex  $\tau$ ,  $k_i = \pm ik_0$  are also resonances of their respective potential  $V_{\pm}(x)$  where  $\tau$  becomes  $1/k_i$ , and hence  $\pm ik_0$  can be treated as two imaginary "siblings" of the active resonance at  $k_0$ . In the case that w(x) is a linear function of x (see Fig. 2), the imaginary sibling at  $ik_0$  also corresponds to the ground state of the quantum harmonic oscillator [see Supplemental Material, Eq. (S21) [27]].

While an active resonance exists for an arbitrary continuous function  $w(x) \in \mathbb{R}$  that satisfies the outgoing boundary condition, the particular  $w(x) = n_e x/a$  used in Fig. 2 leads to a constant  $\mathrm{Im}[\varepsilon_w(x)] \propto w'(x)$ , i.e., a spatially uniform gain that is convenient to implement experimentally. To propose a realistic cavity design where an active resonance can be observed, we also note the inherent challenge imposed by the outgoing boundary condition  $w(\pm a) = \pm n_e$ . It requires the continuous function w(x) to be zero at some point(s) inside the cavity, which means that  $\varepsilon_r(x)$  needs to vanish at these point(s) as well. This stringent condition can be fulfilled by utilizing the effective (instead of the intrinsic) dielectric function, and here we consider a realization using an elongated bow-tie cavity.

As shown in Fig. 3(a), the width s(x) of the cavity is tapered toward its center,

$$s(x) = \frac{\pi}{k_0} \left[ \varepsilon_0 - \frac{n_e^2 x^2}{a^2} \right]^{-1/2},$$
 (9)

with the cutoff frequency at its waist equal to the target frequency of the active resonance. This configuration leads to the same effective dielectric function for the active resonance as in the 1D model discussed above, i.e.,  $\varepsilon_{\rm eff} = \varepsilon - k_y^2(x)/k_0^2 = n_e^2 x^2/a^2 - i\varepsilon_1$ , with  ${\rm Re}[\varepsilon_{\rm eff}] = 0$  at x=0 [solid line, Fig. 3(b)].  $\varepsilon = \varepsilon_0 - i\varepsilon_1(\varepsilon_{0,1}>0)$  is the intrinsic dielectric constant with gain, and  $k_y(x) = \pi/s(x)$  is the position-dependent transverse wave vector. Here we have imposed the Dirichlet boundary condition on the side walls, which can be implemented using a silver coating with a dielectric spacing layer to mitigate the metallic loss [42,43]. Outside the cavity s(x) = s(a) is a constant (i.e., a waveguide), where the effective refractive index is given by  $n_e = [\varepsilon_0 - k_y^2(a)/k^2]^{1/2}$ .

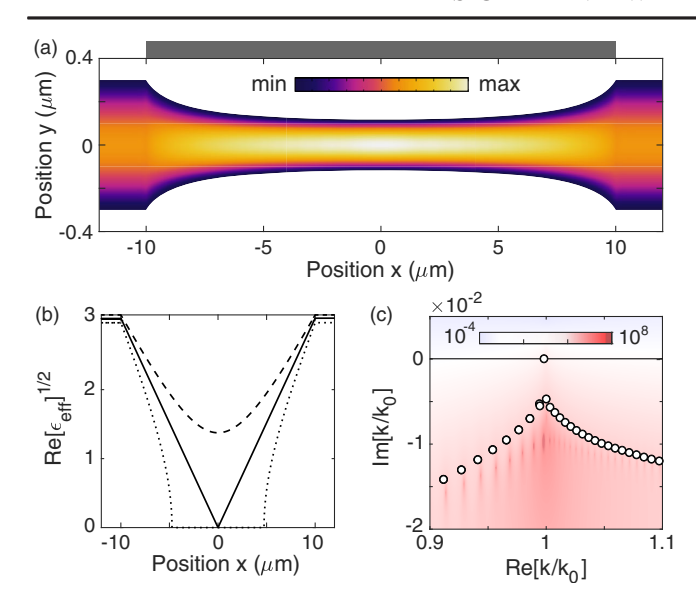


FIG. 3. (a) Proposed bow-tie cavity displaying an active resonance at 1551.0 nm. The color map shows the intensity profile of this active resonance. The spatially uniform gain (shown schematically by the gray box) is at 97.8% of the value predicted by Eq. (6). (b) The effective refractive index for the active resonance in the absence of gain (solid). The dotted and dashed lines show the same for  $\text{Re}[k/k_0] = 0.9$  and 1.1, respectively, with higher average values. (c) The distribution of the resonances in the complex plane. Dots are the simulation result and the background shows det *S* in the logarithmic scale obtained from the 1D effective model.

With a target free-space wavelength of 1550 nm, we use InGaAsP quantum wells as the cavity material [18]. Equation (6) then predicts a required gain  $\varepsilon_i = n_e/k_0 a =$  $7.49 \times 10^{-2}$  in order to observe the active resonance in a bow-tie cavity with  $L=20 \mu m$ ,  $y(a)=0.6 \mu m$ , and  $\varepsilon_0 = 10.89$ . The finite-element simulation agrees well with this analytical result, and the active resonance is found at 1551.0 nm and 97.8% of the expected gain level. We note that this laser threshold is comparable to a ridge waveguide laser [see Eq. (S25) in Ref. [27]]. Its wave function is shown in Fig. 3(a), which displays the fundamental transverse mode both inside and outside the cavity. Although its amplitude along the axial direction is not a constant inside the cavity, as Eq. (7) shows, it still varies slowly to justify the WKB approximation that leads to Eq. (2), based on which we have identified the active resonance. This feature suppresses undesired spatial hole burning [44], and together with the striking "\lambda" distribution of passive resonances shown in Fig. 3(c), it leads to a robust singlemode performance as verified by the steady-state ab initio laser theory [45–47] in the nonlinear regime (see Supplemental Material, Fig. S10 [27]).

To tune the frequency of the active resonance via the gain, we keep the cavity shape unchanged and denote the shifted active resonance simply by k. For simplicity, below we assume that the material dispersion is much weaker than

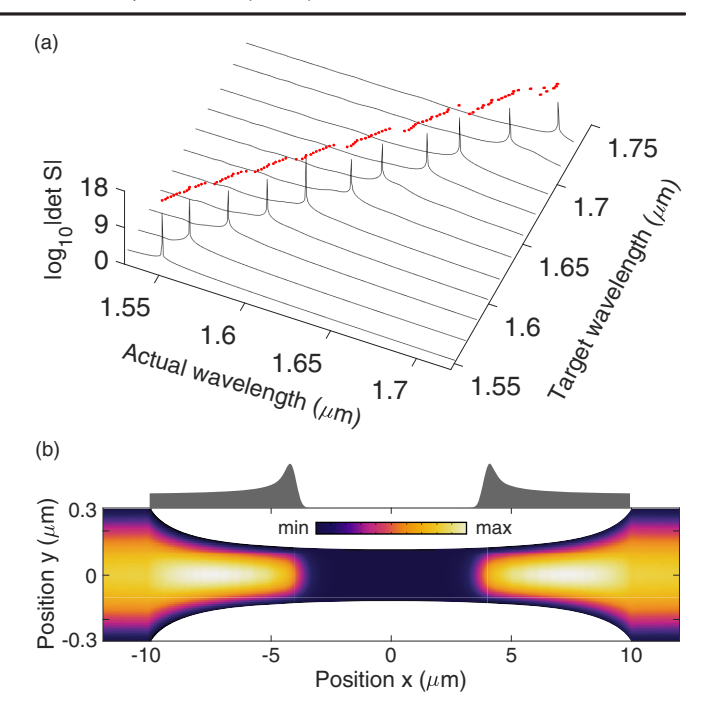


FIG. 4. Tuning the wavelength of the active resonance. (a) Its actual wavelength versus the target wavelength (red dots). Lines exemplify det S that diverges at each shifted active resonance. (b) Intensity profile of the active resonance at 1657.9 nm. The color scale is the same as in Fig. 3(a). The corresponding gain profile proportional to  $-\text{Im}[\varepsilon_{\text{eff}}]$  in the effective cavities is shown schematically as gray shaded areas.

the geometry-induced dispersion in  $\varepsilon_{\rm eff}(x;k)$  and neglect the former. This geometry-induced dispersion alters the form of w(x) for the shifted active resonance: It is now given by  $w_{\rm eff}^2(x;k) \equiv {\rm Re}[\varepsilon_{\rm eff}(x;k)]$ . When  ${\rm Re}[k]$  is greater than the original target frequency  $k_0$ , we observe that  $Re[\varepsilon_{eff}(x;k)]$  has no node inside the cavity [see, for example, the dashed line in Fig. 3(b)]. Therefore, a continuous  $w_{\text{eff}}(x; k)$  with node(s) required by the active resonance cannot be defined. To avoid this problem, our tuning strategy is then to choose  $Re[k] < k_0$ , i.e., redshift the active resonance. As a result, light is now below the cutoff frequency of the fundamental transverse mode in the middle section of the bow-tie cavity, and hence it cannot propagate. In other words, an (almost) impenetrable potential barrier now exists near x = 0 in the WKB analysis (cf. Fig. S3 in Ref. [27]), creating two effective cavities [see Fig. 4(b)]. Note that a passive resonance blueshifts when the cavity length is reduced, in general, while the active resonance here shows the opposite behavior.

Because of the replacement of w(x) by  $w_{\rm eff}(x;k)$ , the spatial distribution of the gain required by the shifted active resonance needs to be adjusted to be proportional to  $w'_{\rm eff}(x;k)$ , which can be achieved, e.g., via a spatial light modulator [48–52] when the laser is pumped optically. Here we only supply gain in the two effective cavities. Although  $w'_{\rm eff}(x;k)$  diverges at the inner edges of these

effective cavities [see Eq. (S31) in Ref. [27]], we find that the active resonance is retained on the real axis by smoothing  $w'_{eff}(x;k)$  with a Gaussian function, accompanied by adjusting the strength of the gain accordingly. This robustness against shape perturbation of the gain profile allows us to achieve semicontinuous tuning of the active resonance shown by the red dots in Fig. 4(a): It is tuned from 1551 to 1711 nm and follows closely the designed range of [1550, 1722] nm. The range is determined by the maximal level of achievable gain density, which we assume to be 9.2 times that at  $k_{\text{max}}$ . The waterfall plot exemplifies the diverging value of det S at the active resonance on the real axis, indicating good single-mode performance. The spatial profile of the active resonance at 1657.9 nm and the supplied gain are plotted in Fig. 4(b), showing the two effective cavities and the barrier region in between. We note that such a semicontinuous tuning is not due to selective pumping that favors different passive resonances, which would lead to mode hopping (see Supplemental Material, Fig. S9 [27]).

In summary, we have identified a new resonance condition by analyzing the non-Hermitian extension of the WKB analysis with a complex dielectric function. When the real and imaginary parts of the latter are spatially correlated according to Eq. (6), an active resonance is found on the real frequency axis that does not originate from a passive counterpart. Its signature redshift upon the increase of optical gain has also been verified in an elongated bowtie cavity, which is robust against shape deformation that may occur during fabrication (see Sec. IV in Ref. [27]). Although the simulations we have presented are two dimensional, we do not expect additional conceptual challenges in three dimensions. From a practical perspective, this new active resonance enables an innovative frequency tuning strategy in laser technology, delivering an ultrawide-range tunable semiconductor laser. The continuous tuning range is expected to be enhanced by 1-2 orders of magnitude by this strategy when compared to the state-of-the-art on-chip lasers, such as distributed feedback lasers and distributed Bragg reflector lasers [53,54].

L. G. acknowledges support by the National Science Foundation (NSF) under Grant No. PHY-1847240. L. F. acknowledges support by Army Research Office (ARO) under Grant No. W911NF-19-1-0249 and NSF under Grant No. ECCS-1846766.

- [3] D. Kleppner, Inhibited Spontaneous Emission, Phys. Rev. Lett. 47, 233 (1981).
- [4] P. Goy, J. M. Raimond, M. Gross, and S. Haroche, Observation of Cavity-Enhanced Single-Atom Spontaneous Emission, Phys. Rev. Lett. 50, 1903 (1983).
- [5] G. Gabrielse and H. Dehmelt, Observation of Inhibited Spontaneous Emission, Phys. Rev. Lett. 55, 67 (1985).
- [6] T. J. Kippenberg, A. L. Tchebotareva, J. Kalkman, A. Polman, and K. J. Vahala, Purcell-Factor-Enhanced Scattering from Si Nanocrystals in an Optical Microcavity, Phys. Rev. Lett. 103, 027406 (2009).
- [7] D. Meschede, H. Walther, and G. Müller, One-Atom Maser, Phys. Rev. Lett. 54, 551 (1985).
- [8] E. T. Jaynes and F. W. Cummings, Comparison of quantum and semiclassical radiation theories with application to the beam maser, Proc. IEEE **51**, 89 (1963).
- [9] J. H. Eberly, N. B. Narozhny, and J. J. Sanchez-Mondragon, Periodic Spontaneous Collapse and Revival in a Simple Quantum Model, Phys. Rev. Lett. 44, 1323 (1980).
- [10] W. Jhe, A. Anderson, E. A. Hinds, D. Meschede, L. Moi, and S. Haroche, Suppression of Spontaneous Decay at Optical Frequencies: Test of Vacuum Field Anisotropy in Confined Space, Phys. Rev. Lett. 58, 666 (1987).
- [11] M. O. Scully, B. G. Englert, and H. Walther, Quantum optical tests of complementarity, Nature (London) **351**, 111 (1991).
- [12] Y. Yamamoto and R.E. Slusher, Optical processes in microcavities, Phys. Today **46**, No. 6, 66 (1993).
- [13] J. M. Fink, M. Gppl, M. Baur, R. Bianchetti, P. J. Leek, A. Blais, and A. Wallraff, Climbing the Jaynes-Cummings ladder and observing its nonlinearity in a cavity QED system, Nature (London) 454, 315 (2008).
- [14] R. J. Schoelkopf and S. M. Girvin, Wiring up quantum systems, Nature (London) **451**, 664 (2008).
- [15] S. Haroche, Nobel Lecture: Controlling photons in a box and exploring the quantum to classical boundary, Rev. Mod. Phys. **85**, 1083 (2013).
- [16] C. W. Hsu, B. Zhen, A. D. Stone, J. D. Joannopoulos, and M. Soljačić, Bound states in the continuum, Nat. Rev. Mater. 1, 16048 (2016).
- [17] R. E. Peierls, Complex eigenvalues in scattering theory, Proc. R. Soc. A **253**, 16 (1959).
- [18] L. Feng, R. El-Ganainy, and L. Ge, Non-Hermitian photonics based on parity-time symmetry, Nat. Photonics 11, 752 (2017).
- [19] R. El-Ganainy, K.G. Makris, M. Khajavikhan, Z.H. Musslimani, S. Rotter, and D.N. Christodoulides, Non-Hermitian physics and *PT* symmetry, Nat. Phys. 14, 11 (2018).
- [20] P. Miao, Z. Zhang, J. Sun, W. Walasik, S. Longhi, N. M. Litchinitser, and L. Feng, Orbital angular momentum microlaser, Science 353, 464 (2016).
- [21] Z. Zhang, X. Qiao, B. Midya, K. Liu, J. Sun, T. Wu, W. Liu, R. Agarwal, J. M. Jornet, S. Longhi, N. M. Litchinitser, and L. Feng, Tunable topological charge vortex microlaser, Science 368, 760 (2020).
- [22] B. Peng, Ş. K. Özdemir, M. Liertzer, W. Chen, J. Kramer, H. Ylmaz, J. Wiersig, S. Rotter, and L. Yang, Chiral modes and directional lasing at exceptional points, Proc. Natl. Acad. Sci. U.S.A. 113, 6845 (2016).

<sup>\*</sup>These two authors contributed equally to this work.
†fenglia@seas.upenn.edu

<sup>‡</sup>li.ge@csi.cuny.edu

<sup>[1]</sup> A. E. Siegman, Laser beams and resonators: Beyond the 1960s, IEEE J. Sel. Top. Quantum Electron. 6, 1389 (2000).

<sup>[2]</sup> E. M. Purcell, H. C. Torrey, and R. V. Pound, Resonance absorption by nuclear magnetic moments in a solid, Phys. Rev. 69, 37 (1946).

- [23] L. Ge, Y. D. Chong, S. Rotter, H. E. Türeci, and A. D. Stone, Unconventional modes in lasers with spatially varying gain and loss, Phys. Rev. A 84, 023820 (2011).
- [24] R. El-Ganainy, M. Khajavikhan, and L. Ge, Exceptional points and lasing self-termination in photonic molecules, Phys. Rev. A **90**, 013802 (2014).
- [25] M. Brandstetter, M. Liertzer, C. Deutsch, P. Klang, J. Schöberl, H. E. Türeci, G. Strasser, K. Unterrainer, and S. Rotter, Reversing the pump dependence of a laser at an exceptional point, Nat. Commun. 5, 4034 (2014).
- [26] B. Peng, Ş. K. Özdemir, S. Rotter, H. Yilmaz, M. Liertzer, F. Monifi, C. M. Bender, F. Nori, and L. Yang, Loss-induced suppression and revival of lasing, Science 346, 328 (2014).
- [27] See Supplemental Material at http://link.aps.org/supplemental/10.1103/PhysRevLett.126.163901 for more discussions and examples, which includes Refs. [28–30].
- [28] C. M. Bender and S. Boettcher, Real Spectra in Non-Hermitian Hamiltonians Having PT Symmetry, Phys. Rev. Lett. 80, 5243 (1998).
- [29] C. M. Bender, S. Boettcher, and P. N. Meisinger, PT-symmetric quantum mechanics, J. Math. Phys. (N.Y.) 40, 2201 (1999).
- [30] L. Ge, Y. D. Chong, and A. D. Stone, Conservation relations and anisotropic transmission resonances in one-dimensional PT-symmetric photonic heterostructures, Phys. Rev. A 85, 023802 (2012).
- [31] G. C. Wick, Properties of Bethe-Salpeter wave functions, Phys. Rev. 96, 1124 (1954).
- [32] S. Weinberg, *The Quantum Theory of Fields* (Cambridge University Press, Cambridge, 2005), Vol. III.
- [33] https://www.rp-photonics.com/wavelength\_tuning.html (accessed Jan. 15, 2021).
- [34] https://www.rp-photonics.com/distributed\_bragg\_reflector\_lasers.html (accessed Jan. 15, 2021).
- [35] Y. D. Chong, L. Ge, H. Cao, and A. D. Stone, Coherent Perfect Absorbers: Time-Reversed Lasers, Phys. Rev. Lett. 105, 053901 (2010).
- [36] D. J. Griffiths, Introduction to Quantum Mechanics, 2nd ed. (Cambridge University, New York, 2016).
- [37] G. P. Agrawal, J. E. Geusic, and P. J. Anthony, Distributed feedback lasers with multiple phase-shift regions, Appl. Phys. Lett. **53**, 178 (1988).
- [38] T. Schrans and A. Yariv, Semiconductor lasers with uniform longitudinal intensity distribution, Appl. Phys. Lett. 56, 1526 (1990).
- [39] K. G. Makris, Z. H. Musslimani, D. N. Christodoulides, and S. Rotter, Constant-intensity waves and their modulation instability in non-Hermitian potentials, Nat. Commun. 6, 7257 (2015).

- [40] K. G. Makris, A. Brandstötter, P. Ambichl, Z. H. Musslimani, and S. Rotter, Wave propagation through disordered media without backscattering and intensity variations, Light 6, e17035 (2017).
- [41] E. Rivet, A. Brandstötter, K. G. Makris, H. Lissek, S. Rotter, and R. Fleury, Constant-pressure sound waves in non-Hermitian disordered media, Nat. Phys. 14, 942 (2018).
- [42] M. P. Nezhad, A. Simic, O. Bondarenko, B. Slutsky, A. Mizrahi, L. Feng, V. Lomakin, and Y. Fainman, Room-temperature subwavelength metallo-dielectric lasers, Nat. Photonics 4, 395 (2010).
- [43] A. Mizrahi, V. Lomakin, B. A. Slutsky, M. P. Nezhad, L. Feng, and Y. Fainman, Low threshold gain metal coated laser nanoresonators, Opt. Lett. 33, 1261 (2008).
- [44] Z. Zhang, P. Miao, J. Sun, S. Longhi, N. M. Litchinitser, and L. Feng, Elimination of spatial hole burning in microlasers for stability and efficiency enhancement, ACS Photonics 5, 3016 (2018).
- [45] H. E. Türeci, L. Ge, S. Rotter, and A. D. Stone, Strong interactions in multimode random lasers, Science 320, 643 (2008).
- [46] L. Ge, Y. D. Chong, and A. D. Stone, Steady-state *ab initio* laser theory: Generalizations and analytic results, Phys. Rev. A 82, 063824 (2010).
- [47] L. Ge, O. Malik, and H. E. Türeci, Enhancement of laser power-efficiency by control of spatial hole burning interactions, Nat. Photonics 8, 871 (2014).
- [48] M. Leonetti and C. López, Active subnanometer spectral control of a random laser, Appl. Phys. Lett. 102, 071105 (2013).
- [49] S. F. Liew, B. Redding, L. Ge, G. S. Solomon, and H. Cao, Active control of emission directionality of semi-conductor microdisk lasers, Appl. Phys. Lett. 104, 231108 (2014)
- [50] T. Gao et al., Observation of non-Hermitian degeneracies in a chaotic exciton-polariton billiard, Nature (London) 526, 554 (2015).
- [51] S. Schönhuber, N. Bachelard, B. Limbacher, M. A. Kainz, A. M. Andrews, H. Detz, G. Strasser, J. Darmo, S. Rotter, and K. Unterrainer, All-optical adaptive control of quantum cascade random lasers, Nat. Commun. 11, 5530 (2020).
- [52] J. D. Töpfer, I. Chatzopoulos, H. Sigurdsson, T. Cookson, Y. G. Rubo, and P. G. Lagoudakis, Engineering spatial coherence in lattices of polariton condensates, Optica 8, 106 (2021).
- [53] https://www.thorlabs.com/newgrouppage9.cfm?objectgroup \\_id=9024 (accessed Jan. 15, 2021).
- [54] https://www.photonics.com/Products/DFB\\_TUNABLE\\_ LASER/pr17931 (accessed Jan. 15, 2021).